Distribution of Dust Color Temperature, Planck's Function and Dust Mass around PSR J1240-4124

Ashok Chaudhary, Bikash Thapa, Tapendra Sodari, Keshab Chaudhary and Devendra Raj Upadhyay

Journal of Nepal Physical Society
Volume 8, No 1, 2022
(Special Issue: ICFP 2022)
ISSN: 2392-473X (Print), 2738-9537 (Online)

JNPS, **8** (1), 88-95 (2022)
DOI: http://doi.org/10.3126/jnphyssoc.v8i1.48292

Published by: Nepal Physical Society
P.O. Box: 2934
Tri-Chandra Campus
Kathmandu, Nepal
Email: nps.editor@gmail.com

ICFP 2022
ISSN:2392-473X (Print)
2738-9537 (Online)

Research Article ©Nepal Physical Society
DOI:http://doi.org/10.3126/jnphyssoc.v8i1.48292

Distribution of Dust Color Temperature, Planck's Function, and Dust Mass around PSR J1240-4124

Ashok Chaudhary,[1, 2, a)] Bikash Thapa,[1] Tapendra Sodari,[2] Keshab Chaudhary,[1] and Devendra Raj Upadhyay[1, b)]

[1)] *Central Department of Physics, Tribhuvan Univeristy, Nepal*
[2)] *Department of Physics, Amrit Campus, Tribhuvan University, Nepal*

[a)] *Electronic mail: ashok.775511@cdp.tu.edu.np*
[b)] *Corresponding author: devendra.upadhyay@ac.tu.edu.np*

Abstract. The dust properties in the interstellar medium play an important role in structure formation and extinction of high-energy radiation. This study performed an investigation of the physical properties like distribution of dust color temperature, Planck's function, and dust mass of the cavity around the pulsar PSR J1240-4124 in the IRIS and the AKARI surveys. In our study, the dust color temperature in the IRIS survey is found to be in the range of 23.607 $\pm$ 0.012 K to 24.342 $\pm$ 0.012 K with an offset of 0.735 K. Such low offset temperature indicates that the isolated cavities are in thermal equilibrium. In the case of the AKARI survey, the dust temperature was found to be in the range of 16.123 $\pm$ 0.017 K to 18.802 $\pm$ 0.017 K with an offset of 2.679 K. The average dust mass in IRIS survey is found to be 2.1 $\times$ 10^{-4} $M_{\odot}$ and that of the AKARI is 8.1$\times$ 10^{-4} $M_{\odot}$. The size of the structure in the IRIS map is 14.62 pc $\times$ 6.24 pc and that of the AKARI map is 5.80 pc $\times$ 0.17 pc. The angle of inclination for the selected cavity region is found to be 73.330° in IRIS and that of AKARI is 110.260°. We have tried to present the relationship among the different physical parameters and compare the results in the IRIS and the AKARI surveys. Our findings are similar to those obtained in previous studies of other cavity structures around pulsars. This confirms the validity of the existing results for a new cavity around PSR J1240-412.

Received: 11 March 2022; **Revised**: 12 April 2022; **Accepted**: 3 May 2022

Keywords: ISM, Dust Color Temperature, Dust Mass, Inclination angle, Extinction.

INTRODUCTION

Rotating Neutron stars are formed from the explosion of massive stars (8-25) known as a supernova explosion. During the phase of the supernova, the star explodes and the core collapses and resulting in to a neutron star [1]. The charged particles in Neutron stars travel at relativistic speeds, causing many types of radiation to be produced. Because neutron stars' spinning and magnetic axes do not align with each other, radio waves are emitted from the region between their magnetic and spinning axes. We can observe a pulse of radio wave if these radio beams pass by Earth in our line of sight. We detect pulses of radiation as a result of these sweeping lighthouse-like beams across our line of sight, which is why they're called pulsars [2] [3]. The interstellar medium (ISM) of the galaxy has a complicated distribution of cavities, filaments, arcs, loops, lobes, and shells at a massive scale and the study of the creation of Galactic shells was happen due to Supernova explosions and powerful stellar winds [4].

Bubbles and super bubbles produced by supernova explosions and high-pressure events, such as strong stellar wind released from star associations, are thought to govern the evolution of these formations [4]. Gas and dust structures such as shells, cavities, filaments, arch, and loops are formed due to the explosion of a star. These structures are ruled by the bubble and super bubbles produced by the supernova explosion and high-pressure events(citation). Hydrogen is the prominent component in ISM in different forms: Molecular forms(H_2), Neutral forms, and ionized form(HII) [5]. Dust in ISM absorbs and re-emits the ultraviolet radiation in the infrared band. The study of dust in ISM is important because it controls the chemistry and thermal process and the formation of earth-like planets [6].

Jha et al. performed a study of dust color temperature and dust mass distribution of four infrared loops. They calculated the dust color temperature, dust mass, and inclination angle of four infrared loops namely G007+18, G1414+07, G214-01, and G32-02 which are found to be located within 1 0 from pulsar PSR J1270-1633, PSR J0406+6138, PSRJ065-0142, and PSR J1534-5848 respectively. It was found that, except for one KK-loop (G323-02), the dust color temperature and dust mass distribution are very well fitted by the gaussian. In addition to this, they found that the outer regions have higher temperatures, with an offset from 14-20K from that of the core regions [7].

Aryal et al. studied the physical properties of the cavity near pulsar at -60○ latitude. They used far infrared 100μm and 60μm images in AKARI. They found that the dust color temperature varies from 22.75 to 24.78 K with an offset temperature of 2 K. The energy required to create inhomogeneity in the structure is calculated to be 3.24 $\times$ 10^{35}J [8].

Here, we compared the two surveys: IRIS and AKARI, and introduce our work related to the cavity region around the pulsar. This work is based on the Australia Telescope National Facility (ATNF) pulsar database. We have divided our entire work into four parts, the first part is an introduction, the second part is the methodology, the third part is the result and discussion and the fourth part is conclusion.

METHODOLOGY

The ATNF pulsar database was used for getting the names and details of the pulsar including the parameters like name, positions, timing parameters, flux densities, distances, dispersion, and scattering measure. After getting the name of the pulsar, we entered the name in SIMBAD Astronomical Database - CDS (Strasbourg), for getting the coordinates of the given pulsar. We put the coordinates obtained from SIMBAD in Sky View Virtual Observatory. We carried the following steps in Sky View:

Step 1: **Input Parameters**

Coordinates or Source: enter the coordinates resolved from SIMBAD, **Choose the desired survey:** IRIS and AKARI, **Coordinate System:** J2000 (Equatorial Coordinate), **Image Size (pixel):** 500 $\times$ 500, **Image Size (degrees):** 1 $\times$ 1 (for IRAS) and 0.5 $\times$ 0.5 (for AKARI), **Brightness Scaling:** Histogram Equalization, **Color Table:** Stern Special.

Step 2: **Downloading the images:** After including all the parameters, JPEG images were downloaded at different wavelengths 12, 25, 60, and 100 μm in IRIS and 90 and 140μm in AKARI. The FITS(Flexible Image Transport System) images at 60 and 100μm in IRIS and 90 and 140μm in AKARI were downloaded.

Region of Interest

The isolated cavity like structure at R.A. (J2000) = 12^{h} 40^{m} 17.61^{s} Dec. (J2000) = $-41^{\circ}24'51.7''$is the region of interest where we intend to study the physical parameters. The following are the reasons for the selection of this FIR loop:

- The central region of the loop has minima at 100μm in the IRIS map.
- The structure is isolated and the size of the cavity is reasonable and there is no optical diffusion.
- The structure in IRIS is prominent in 60 and 100μm and prominent in 90 and 140μm in AKARI , which facilitates for studying the fluxes emitted from dust and the grain.

Data Reduction

Aladin v2.5 is used for analyzing each pixel of the FITS image in the region of interest. ALADIN is a widely used virtual observatory tool capable of addressing challenges such as locating data of interest, accessing and exploring distributed data sets, and visualizing multi-wavelength data. It is an interactive sky atlas developed and maintained by the Centre de Donnees astronomiques de Strasbourg (CDS) for the identification of astronomical sources through visual analysis of reference sky images. It allows the user to visualize the digitized images of any part of the sky, superimpose entries from the CDS astronomical catalogs and tables, and interactively access related data information from SIMBAD, NED, Vizier, or other archives for all known objects in the field. We aimed to study the cavity like structure at IRIS 60 μm and 100 μm and AKARI WIDE-S and AKARI WIDE-L.

WORKING FORMULA

Dust Color Temperature

The dust color temperature was calculated using the Dupac et al. and Schnee et al. [9] [10]methods. The following assumptions can be used to calculate the dust color temperature, T_d, in each pixel of the FITS image.

- Each single beam of dust is isothermal.
- The observed ratio of 60 and 100 μm is due to black body radiation from dust grains at T_d, adjusted by a power law of spectral emissivity index.

The expression for the dust color temperature in IRIS survey is given by

$$T_d = \frac{-96}{\ln[R \times 0.6^{(3+\beta)}]} \quad (1)$$

Where flux density ratio, R, is given by

$$R = \frac{F_{(60\mu m)}}{F_{(100\mu m)}} \quad (2)$$

The flux densities at 60 and 100μ, respectively, are F(60μ) and F(100μ). The spectral emissivity index value,β, is determined by dust particle parameters such as composition, size, and compaction. A pure black substance has a value of β=0, amorphous layer lattice matter has a value of β=1, and crystalline dielectric has a value of β=2. The expression for dust color temperature in the AKARI survey is,

$$T_d = \frac{-57}{\ln[R \times 0.6^{(3+\beta)}]} \quad (3)$$

Where flux density ratio, R, is given by

$$R = \frac{F_{(90\mu m)}}{F_{(140\mu m)}} \quad (4)$$

Here, $F_{(90\mu m)}$ and $F_{(140\mu m)}$ are the flux densities at 90 μm and 140 μm respectively [8].

Dust Mass

The IR flux densities are used to calculate the dust mass. The physical and chemical characteristics of the dust grains, the dust color temperature, T_d, and the distance, D, to the object all influence the resultant dust mass [2]. Hilderbrand [11] came up with an empirical method for calculating the dust mass..

$$M_{dust} = \frac{4\alpha\rho}{3Q_\nu}\left[\frac{S_\nu D^2}{B(\nu,T)}\right] \quad (5)$$

where, α = weighted grain size = 0.1 μm, ρ = grain density = 3000 kgm^{-3} ,
Q_ν = grain emissivity = 0.0010 for 100 μm & 60μm, S_ν = total flux density,
S_ν = f $\times$ 5.288$\times 10^{-9}$ MJy/sr, D = distance to the structure, and Planck's function as

$$B(\nu,T) = \frac{2h\nu^3}{c^2}\left[\frac{1}{e^{\frac{h\nu}{KT}}-1}\right] \quad (6)$$

Using all the above given values, equation (5) takes the form

$$M_{dust} = 0.4\left[\frac{S_\nu D^2}{B(\nu,T)}\right] \quad (7)$$

Inclination Angle

The inclination angle is the angle between the line of the sight and the plane of the celestial object projected in the sphere. In 1946, Holmberg [10] developed a model to find the inclination angle of the celestial object called Holmberg equation. It is the relation between the axial ratio ($\frac{b}{a}$) and the angle of the inclination (i), the angle between, the angle between the line of the sight and normal to the galactic plane. The flatness factor q* = 0.33 is assumed by considering the oblate spheroid. The Holmberg formula for the calculation of the inclination angle is

$$\cos^2 i = \frac{\frac{b^2}{a^2} - q*^2}{1 - q*^2} \quad (8)$$

RESULTS AND DISCUSSION

Projection Map

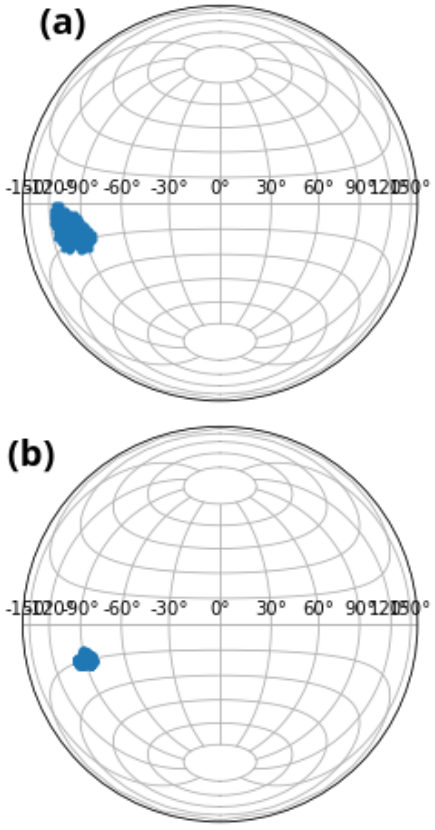

FIGURE 1. Lambert azimuthal equal area map projection (a) IRIS (b) AKARI at RA $12^h\ 40^m\ 17.61^s$ and Dec. at $-41°24'51.7''$

We have used the Lambert Azimuthal Equal Area Projection. Fig .1 (a) and (b), show the map projection of PSR J1240- 4124 in IRIS and AKARI respectively. Here, in this projection map, the candidate is located in the southern hemisphere. It can be seen that the size of the isolated cavity structure in the IRIS is larger than that of the AKARI. The difference in the size of the structure is because we have used $1^\circ \times 1^\circ$ image in the IRIS and $0.5^\circ \times 0.5^\circ$ image in the AKARI.

Hexbin plot of flux distribution

Fig. 2 (a) shows the hexbin of the flux density variation in the IRIS survey at 60μm and Fig. 2 (b) shows the hexbin distribution of Flux density variation in AKARI survey at 90μm. From the hexbin of both the cases, it can be observed that the flux density is higher in the outer regions and moderate amount of flux in the central region while minimum flux in the lower end of our study region which indicates the emitting flux increases from the inner to the outer region.

Contour plot of flux distribution

Fig. 3 (a) shows the contour plot of the flux density distribution in the IRIS survey at 100μm and (b) shows that of the flux density distribution in the AKARI survey at 140μm. From both the contour plot, we can see the presence of green color is dominant over other colors. So, it can be concluded that the majority of the pixels have a moderate amount of flux. The flux density is higher in the outer regions and minimum in the inner region. Here, the flux increases from inner to outer regions. The flux density distribution is higher in the AKARI than that of the IRIS.

Linear Plot of Flux Density

Fig 4 (a) and (b) shows that, in the IRIS map the flux is concentrated toward the center whereas, in the case of the AKARI map, the flux is concentrated slightly toward the left side. For IRIS, we found the slope = 0.218, the correlation coefficient (r)= 0.714, the intercept =0.110 MJy/sr. The positive value of r indicates a positive correlation between the flux densities. Similarly, for the AKARI, we found the slope = -0.098, intercept = 6.868, the correlation coefficient (r)= -0.074. The negative value of r indicates a negative correlation between the flux densities. The best fit lines are,

$$F_{60} = 0.218F_{100} + 0.110 \quad (9)$$

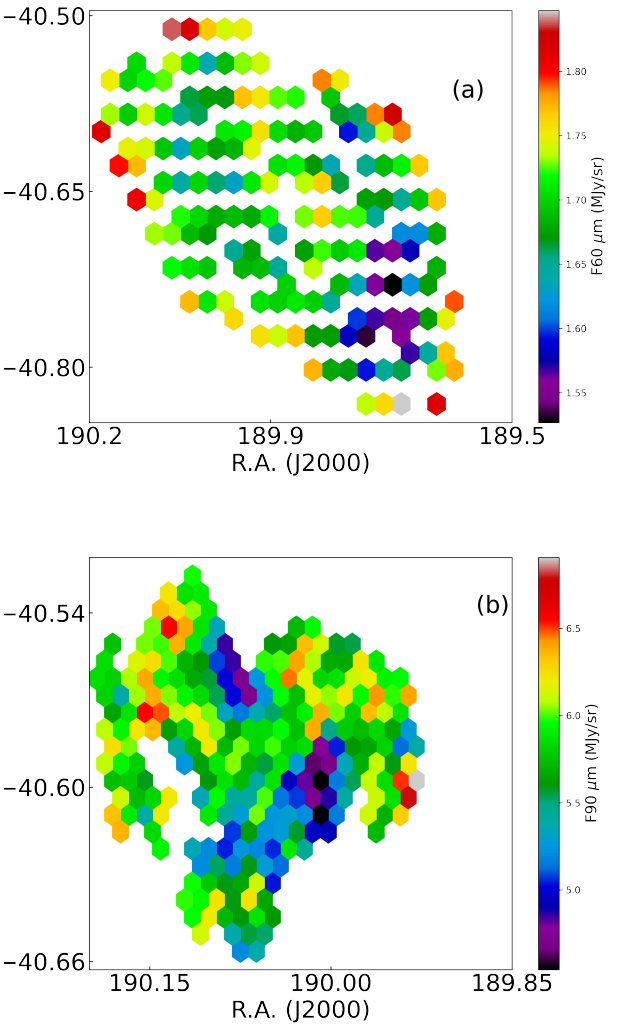

FIGURE 2. Hexbin plot showing the flux density variation in IRIS (a)R.A. vs Dec. vs F60 μm in the IRIS survey (b) R.A. vs Dec. vs F90 μm in the AKARI survey. the flux density. The red color indicates maximum flux region whereas the violet color indicates the minimum flux region.

$$F_{90} = 0.098F_{140} + 6.868 \quad (10)$$

Dust color temperature distribution

The maximum and minimum dust color temperatures in IRIS are found to be 24.342 $\pm$ 0.012 K and 23.608 $\pm$ 0.012 K respectively. The difference in the temperature is 0.282 K. Such a low offset in temperature, T_d , indicates uniform distribution in temperature over the cavity region. Likewise, in AKARI the maximum and minimum value of dust color temperatures are found to be 18.802

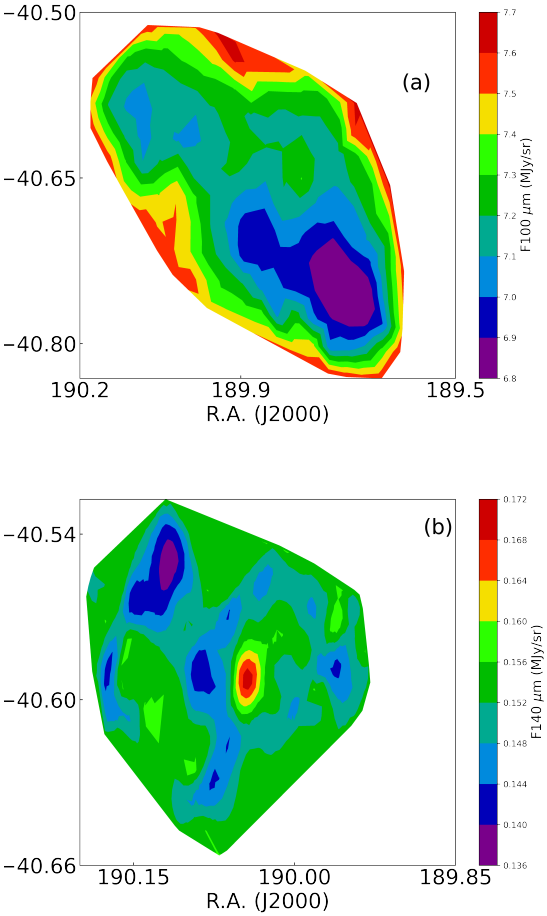

FIGURE 3. Contour plot showing the flux density variation in IRIS (a)R.A. vs Dec. vs F100 μm in IRIS survey (b) R.A. vs Dec. vs F140 μm in AKARI survey. the flux density. The red color indicates maximum flux region whereas the violet color indicates the minimum flux region.

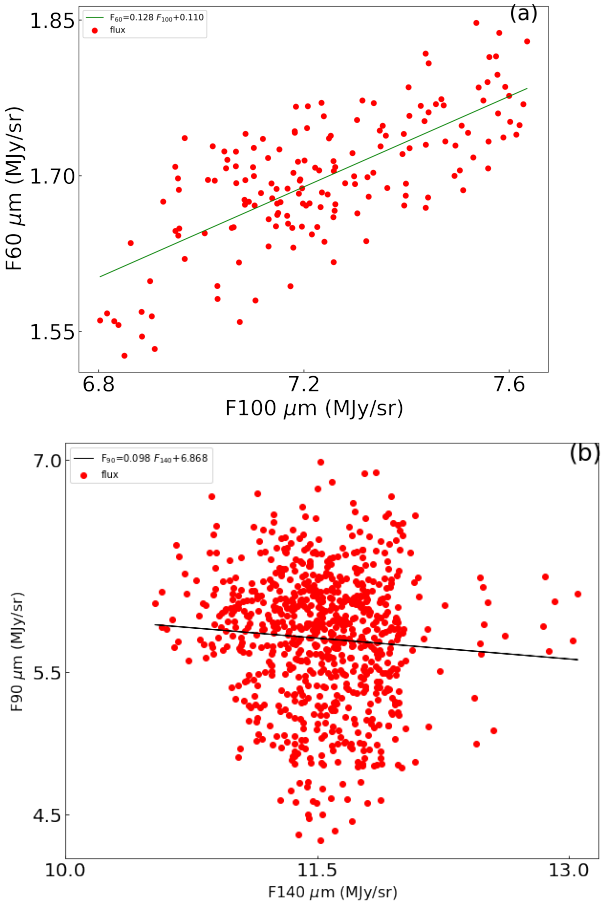

FIGURE 4. Scatter plot with the best fit line between flux density (a) F100μm vs F60μm (b) F140μm vs F90μm. The solid line represents the best fit line whereas the dots represent the flux.

$\pm$ 0.017 K and 16.123 $\pm$ 0.017 K respectively. Here, the offset temperature, T_d, is 2.662 K. Such a low value of T_d indicates that the isolated cavity structure is in thermal equilibrium. The dust color temperature is higher in the case of IRIS than that of AKARI.

Dust mass distribution

Fig. 6 (a) and (b) show the contour plot of distribution of dust color temperature distribution in the IRIS and the AKARI maps respectively. As seen in the contour plot, the maximum and minimum mass in IRIS are found to be 4.643 $\times$ 10^{26} kg and 3.682 $\times 10^{26}$ kg respectively. Similarly, in the case of AKARI, the maximum and minimum values of dust mass distribution are found to be 2.686 $\times$ 10^{27} kg and 1.009 $\times$ 10^{27} kg respectively which can be seen in the contour plot. In both cases, the maximum mass is observed in the outer region, and minimum mass is observed in the inner region which is indicated by the red and the violet color respectively. It can be observed that the value of dust mass is higher in AKARI than that of IRIS.

Planck's function distribution

Fig. 7 (a) and (b) show the contour plot of the Planck's function distribution in the IRIS and AKARI survey respectively. The maximum value of Planck's function lies in the central region in IRIS as indicated by the red color. However, in the AKARI the maximum value of radiation is seen in the upper right region. The radiation is higher

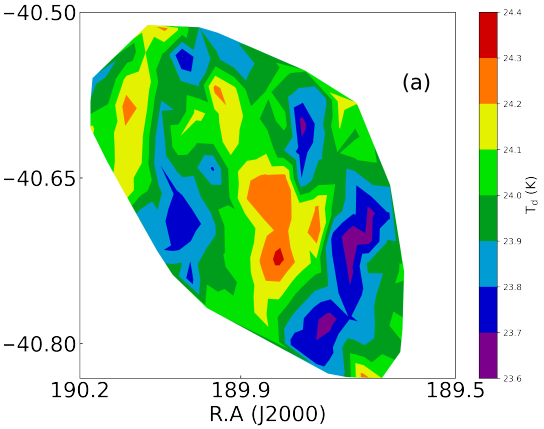

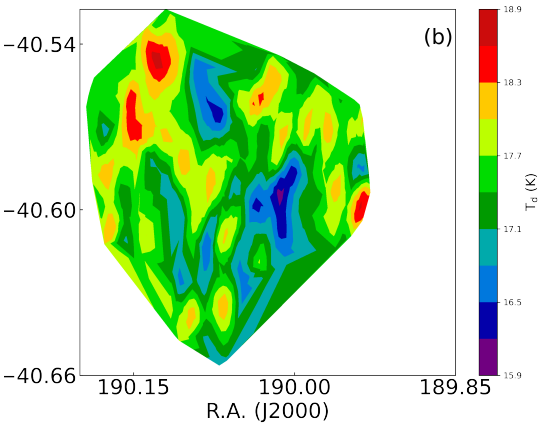

FIGURE 5. Contour plot showing dust color temperature distribution (a) IRIS: RA vs Dec. vs T_d (b) AKARI: RA vs Dec. vs T_d. The color bar indicates the dust color temperature distribution (T_d).

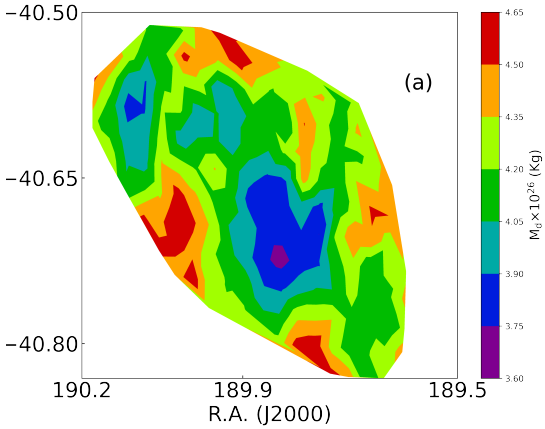

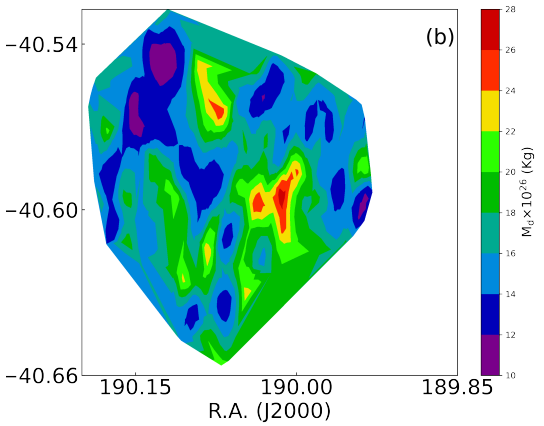

FIGURE 6. Contour plot showing dust mass distribution (a) IRIS: RA vs Dec. vs M_d (b) AKARI: RA vs Dec. vs M_d . Here, M_d is in the range of 10^{26} kg. The color bar indicates the dust mass distribution M_d . The red color and the violet color indicate the maximum and minimum value of dust mass respectively

in the IRIS than that of AKARI.

Size of the structure and inclination angle

We used a simple relation to find the extension and contraction.

$$L = R\theta \tag{11}$$

Where, R is the distance of the candidate (R= 1682 pc) and θ is the angle in radian.

TABLE I. Extension and contraction in IRIS and AKARI

Data map	Contour level	Extension (pc)	Contraction (pc)	Inclination angle
IRIS	20	14.62	6.24	73.33
AKARI	74	5.80	0.17	110.26

COMPARISON WITH PREVIOUS WORK

The above table shows the dust color temperature, dust mass and inclination angle of four far infrared loops namely G007+18, G143+07, G214-01 and G323-02 calculated by Aryal et.al [4]. We also got the similar kinds of results in our calculations.

CONCLUSION

We aimed to study the physical properties of the cavity around the Pulsar. We have selected PSR J1240-4124 for

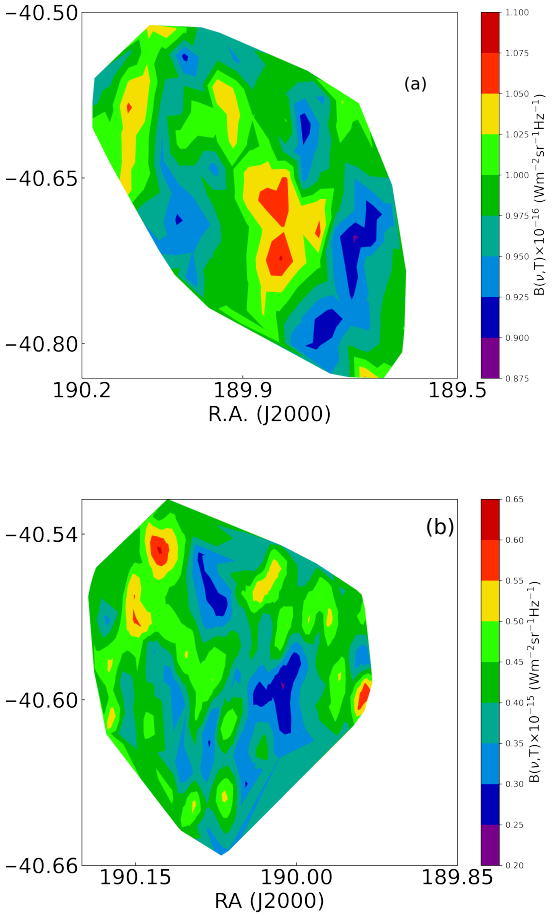

FIGURE 7. Contour plot showing Planck's function distribution (a) IRIS: RA vs Dec. vs B(ν,T) (b) AKARI: RA vs Dec. vs B(ν,T). Here, B(ν,T) is in the range of 10^{-16} $Wm^{-2}sr^{-1}Hz^{-1}$. The color bar indicates the Planck's function distribution B(ν,T).

TABLE II. The inclination angle, dust color temperature and dust mass of the KK-loop. The first columns give the name of the KK-loops.

Name	i (KK) (deg)	i (core) (deg)	T_d (KK) (K)	T_d (core) (K)	M_d(core) ($\times 10^{26}$ kg)
IRAS 04216 +5401	25	83	33.0	19.9	2.96
G143+07	65	76	36.2	23.7	7.42
G214-01	25	71	46.7	19.4	135.04
G323-02	57	72	32.1	25.3	1822.2

our study in the far-infrared region at 60 μm and 100 μm in the IRIS survey and 140 μm and 90 μm in the AKARI survey. We have calculated the dust color temperature, dust mass, size of the structure, and inclination angle. We have studied the flux variation distribution over different parameters.

The dust color temperature of the isolated cavity structure in the IRIS and the AKARI survey is found to be in the range of 23.608$\pm$0.012 K to 24.342 $\pm$ 0.012 K and 16.123 $\pm$0.017 K to 17.524 $\pm$0.017 K, with an offset of 0.282 K and 2.662 K respectively. Such a low value of offset temperature, ΔT_d , indicates a uniform distribution of the temperature of the cavity region. The low value of ΔT_d in both the IRIS and AKARI, suggests that the selected cavity is in the thermal equilibrium. The dust color temperature is found to be higher in the IRIS survey than that of the AKARI survey.

The size of the structure in the IRIS map is found to be 14.62 pc $\times$ 6.24 pc and that of the AKARI is 5.80 pc $\times$ 0.17 pc. The difference in size is due to the use of different pixel images. We have used $1^\circ \times 1^\circ$ images In IRIS and $0.5^\circ \times 0.5^\circ$ images in AKARI. So, we got different sizes of the isolated cavity in the IRIS and the AKARI map.

The maximum value of the dust mass in the IRIS map is found to be 4.274 $\times 10^{-4}$ $M_\odot$ and that of the AKARI map is 2.687 $\times 10^{-4}$ $M_\odot$. There is higher dust mass in the AKARI than that of the IRIS. This is because there is a direct relationship between the dust mass and the wavelength. It also suggests that the distribution of dust mass follows cosmological principle. From the contour plot, it can be seen that the regions having higher temperature have lower mass. Similar work will be done in different bands with different surveys to get more clear understanding about the evolution of these loops.

ACKNOWLEDGMENTS

We wish to acknowledge the support of the author community for constructive analysis and helpful remarks.We would like to acknowledge Australia Telescope National Telescope (ATNF) pulsar database, SIMBAD database, SkyView Virtual Observatory, IRIS survey, AKARI survey

REFERENCES

1. B.Aryal, & R.Weinberger, *Dust Structure Around White Dwarf WD 1003-44 in 60 100 m Iras Survey*, Himalayan Physics, 2, 5-10,(2011).
2. A. K. Jha, and B. Aryal, *A study of a pulsar driven structure in far-infrared IRAS map at latitude -10°*, Journal of Institute of Science and Technology, **22**, 1, 1-9, (2017).
3. Bhattacharya, A. B.; Joardar, S. and Bhattacharya, R. (2008). Astronomy & Astrophysics, Infinity Science Press, India, chapter 19, pp.273.
4. A. K. Jha, B. Aryal, and R. Weinberger, *A study of dust color temperature and dust mass distributions of four far infrared loops*, Rev. Mex. Astron. Astrofis., **53**, 2, (2017).

5. L.Khanal, D. R.,Upadhyay, A. K.,Jha, & , B. Aryal,*Study of ambient environment around Asymptotic Giant Branch Carbon Star: IRAS 01142+6306*,BIBECHANA, **16**, 31–40(2018).
6. M. S.,Paudel, P., Bhandari, & S.Bhattarai,*Study of Dust Cavity around the White Dwarf WD 0352-049 in Infrared Astronomical Satellite Map*, Journal of Nepal Physical Society, 7(2), 110–118, (2021).
7. A. K. Jha, B. Aryal, and R. Weinberger, *A study of dust color temperature and dust mass distributions of four far infrared loops*, Rev. Mex. Astron. Astrofis., **53**, 2, (2017).
8. A . K. Jha, and B. Aryal,*A Study of a Cavity Nearby a Pulsar at-60∘Latitude in the Far Infrared Map*, Journal of Nepal Physical Society,4, 1, 33-41, (2017).
9. X. Dupac, J. P. Bernard, N. Boudet, M. Giard, J. M. Lamarre, C. Mny, F. Pajot, I. Ristorcelli, G. Serra, B. Stepnik, and J.P. Torre, *Inverse Temperature Dependence of the dust sub millimeter spectral index*, Astron. Astrophys, **404**, L11-L15, (2003).
10. S. L. Schnee, N. A. Ridge, A. A. Goodman, and G. L. Jason, *A Complete Look at The Use of IRAS Emission Maps to Estimate Extinction and Dust Temperature*, Astrophys. J., **634**, 442- 450, (2005).
11. R. H. Hildebrand, *The determination of cloud masses and dust characteristics from submillimetre thermal emission*, Q. J. R. Astron. Soc., **24**, 267, (1983).
12. B. A. Bodhaine, N. B. Wood, E. G. Dutton, and J. R. Slusser, *On Rayleigh optical depth calculations*, J. Atmos. Oceanic Technol., **16**, 11, 1854-1861, (1999).
13. E. Holmberg, *On the apparent diameters and the orientation in space of extragalactic Nebulae*, Meddelanden fran Lunds Astronomiska Observatorium Serie II, **117**, 3-82, (1946).
14. R. J. Trumpler, *Preliminary results on the distances, dimensions and space distribution of open star clusters*, Lick Observatory Bulletin, **14**, 154-188, (1930).
15. P. Predehl, and J. H. Schmitt, *X-raying the interstellar medium: ROSAT observations of dust scattering halos*, Astron. Astrophys, **293**, 889-905, (1995).
16. T. H. Jarrett, R. L. Dickman, and W. Herbst, *Far-infrared emission in the Rho Ophiuchi region-A comparison with molecular gas emission and visual extinction*, Astrophys. J, **345**, 881-893, (1989).
17. P. C. C. Freire, C. G. Bassa, , N. Wex, I. H. Stairs, D. J. Champion, S. M. Ransom, and F. Camilo, *On the nature and evolution of the unique binary pulsar J1903+ 0327*, MNRAS, **412**, 2763-2780, (2011).
18. R. N. Manchester, G. B. Hobbs, A. Teoh, and M. Hobbs, *The Australia telescope national facility pulsar catalogue*, Astron. J., **129**, 4, 1993, (2005).
19. M. Wenger, F. Ochsenbein, D. Egret, P. Dubois, F. Bonnarel, S. Borde, and R. Monier, *The SIMBAD astronomical database-The CDS reference database foRAstronomical objects*, Astron. Astrophys, **143**, 1, 9-22, (2000).
20. D. Bhattacharya, and E. P. J. van den Heuvel, *Formation and evolution of binary and millisecond radio pulsars*, Phys. Rep., **203**, 1-2, 1-124, (1991).
21. A. Hewish, S.J. Bell, J.D.H. Pilkington, P.F. Scott, R.A. Collins, *Observation of a rapidly pulsating radio source*, Nature, **217**, 709-713, (1968).
22. Y. Gupta, *Pulsars and the ISM*, In Symposium-International Astronomical Union, Cambridge University Press, **199**, 363-368, (2002).
23. D. R.Upadhyay, L. Khanal, P. Hamal, and B.Aryal, *Dust Structure Around Asymptotic Giant Branch Stars*, Proc. Int. Astron. Union, **14**, S343, 525-526,(2018).
24. B. Aryal, *Asymmetric mass-loss from the white dwarf WD 0253+ 209: Secret revealed*, BIBECHANA, **8**, 1-7, (2012).
25. C. A. Beichman, G. Neugebauer, H. J. Habing, P. E. Clegg, T. J. Chester, *Infrared Astronomical Satellite (IRAS) Catalogues and Atlases I: Explanatory Supplement*, US Government Printing Office, Washington, (1988).